ORIGINAL ARTICLE

CrossMark

The effects of voids on structural properties of fused deposition modelled parts: a probabilistic approach

Sigmund A. Tronvoll[1] · Torgeir Welo[1] · Christer W. Elverum[1]

Abstract

In the search to understand the functional capabilities and limitations of fused deposition modelling (FDM) manufactured components, control over their structural behaviour is crucial. For example, voids introduced during the production phase are a large contributor to anisotropy, yet the magnitude of this contribution remains unquantified. As a baseline model for quantifying strength reduction due to process-induced voids, a statistical method for evaluation of the minimum residual (net) cross section is proposed and tested. Our new method serves to predict the reduction in ultimate tensile strength of transversely printed specimens relative to solid or longitudinally printed specimens, based on void sizes identified from microscopy images of the centre plane of a tensile specimen. *ImageJ* is used to identify void sizes from the microscopy images, and residual cross sections are determined using a bit counting *MATLAB* script. From the distribution of residual cross sections, the weakest link for a given sample size is estimated. The accuracy of the proposed method is determined through comparison with experimental test data for samples of polylactic acid (PLA). The results reveal a close yet slightly under-predicted strength estimate, which for the case considered predicted approximately 5 MPa (12%) lower strength than observed in the experiments. Based on our findings, we have established evidence that the anisotropic behaviour of FDM specimens in PLA can to a large extent be explained by the reduction in residual cross section. This implies that other effects such as fracture mechanics and atomic diffusion of polymer chains play a secondary role for the phenomena observed.

1 Introduction

Creating and testing prototypes, as most other experimentation in product development, are mainly an endeavour to reduce uncertainty. How likely is it that the product works as expected? To draw valid conclusions from prototype testing, one would like the performance to be as close to the intended design as possible. This could require compatibility in multiple dimensions, and for physical products, these dimensions could be:

- Appearance
- Dimensions
- Stiffness
- Weight
- Strength

If there are ways in which the prototype performs different than the expected production model, one should at least be aware of the difference and able to estimate the potential deviation [1].

A major topic for prototyping processes over the past several years, probably boosted by the maker-movement, has been additive manufacturing (AM). Moreover, due to technology advances and patent expirations, AM has now become affordable for many hardware designers and engineers. For many cases, this technology has reduced the need of going

---

✉ Sigmund A. Tronvoll
sigmund.tronvoll@ntnu.no

1 Department of Mechanical and Industrial Engineering, NTNU - Norwegian University of Science and Technology, Richard Birkelands vei 2B, 7491 Trondheim, Norway

through production drawings and highly skilled labour to produce and hence test complex parts. Especially for production components such as injection moulded plastics, it is now possible to generate close-to-final quality-products by "hitting a button" and letting time do the work.

The industry surveying Wohlers Report shows that the volume of AM machines is largely driven by sales of consumer-directed machines, sold not only to consumers, but also to industrial customers. In 2015, an estimate of almost 280,000 desktop printers (sub 5000$) were sold worldwide, compared to approximately 13,000 units in the industrial price range [2]. Currently, the consumer segment is dominated by a single process type—namely the fused deposition modelling—in which lines of heated thermoplastic (called filament) are deposited, fused together and stacked in layers [3].

However, this filament fusing layer depositing method does create several compatibility issues. For the dimensions and appearance, one is restricted by the filament widths and layer heights, giving a minimum shell thickness and a clear "layered" look. While for the mechanical performance, one must tune the build strategy, process parameters and material to achieve the desired behaviour. Therefore, significant effort is put into investigating how these factors affect the mechanical performance.

The most apparent topic for investigation of mechanical strength of FDM parts is the change of tensile capacity for different build strategies, pioneered by the work of Ahn, Montero, Odell, Roudy and Wright [4, 5], as well as the investigation of the mesostructure by Rodríguez, Thomas and Renaud [6, 7]. The anisotropy arises from the fact that the load-bearing capacity of a filament along its axis of deposition differs from the capacity transversely of two filaments melted together (inter filament bonding). Optimization of process
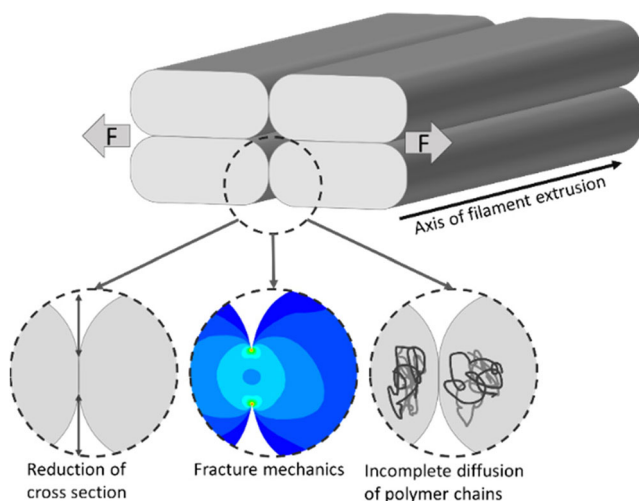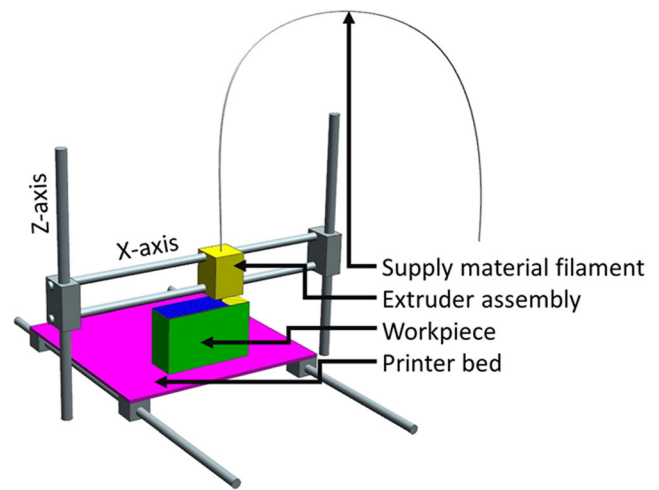

Fig. 2 3D printer axis and components

parameters and strategies to reduce this anisotropy—or generally increase the mechanical strength—has therefore been a major topic among researchers [8–15].

Our research started off likewise, aiming to reduce the anisotropy through annealing. This has proven to be effective for inter filament bonding in an earlier scientific study [8], but also been debated in different forums of the 3D printing community. The basic concept is that, when trying to melt together two lines of filament, one gets a reduction in strength compared to the bulk material due to incomplete diffusion of polymer chains, reduced cross section (introducing voids) and fracture mechanics type stress concentrations, as seen in Fig. 1. Annealing was therefore introduced to increase atomic diffusion. However, initial tests indicated no effect on the tensile specimens in polylactic acid (PLA). As a result, the following question was raised: What is the baseline reduction in strength due to each mechanism? There are numbers of papers seeking to improve the FDM process [8, 12–14, 16], yet, very few quantify the potential performance increase due to their proposed process enhancements.

To better understand the performance of 3D-printed parts, unlike process optimization where one seeks to find the optimal process parameters, we would therefore try to answer the
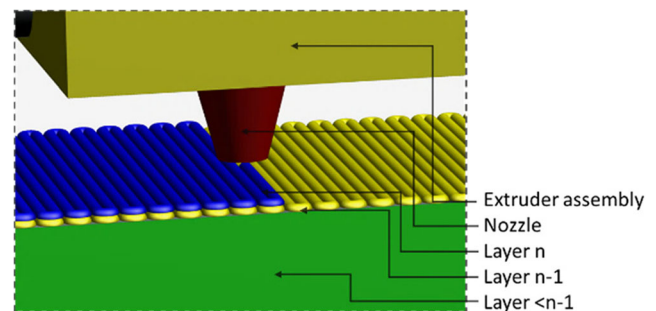

Fig. 1 The three main inter filament bonding strength reduction mechanisms. F denotes load direction

Fig. 3 Close-up of print paths with no perimeter. Colour for contrast only. Only two last layers shown, for convenience
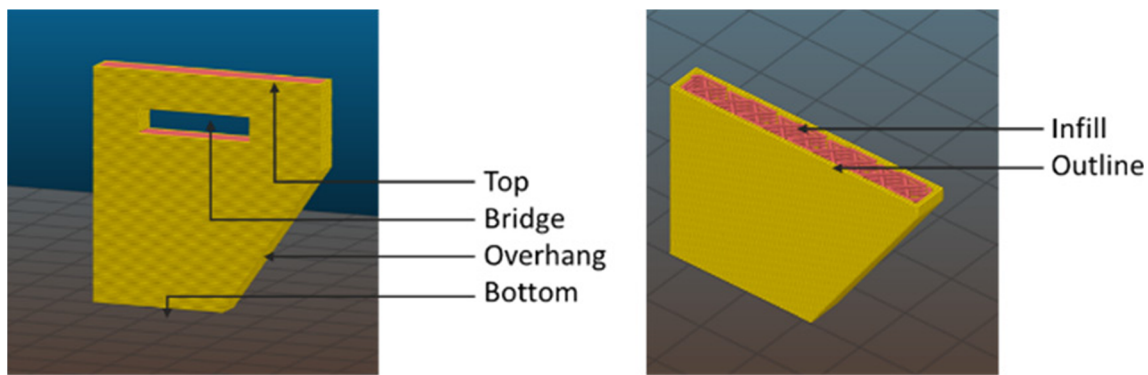
Fig. 4 Different area/volume domains of 3D-printed parts

following question: Just by visually inspecting the 3D-printed specimen, what can we expect of strength reduction due to the reduction in cross section, resulting from the characteristics of the process?

As a starting point, we propose a simple engineering method to estimate the nominal reduction in tensile strength due to voids. The method is meant to predict failure stress of transversely infilled tensile specimens, based on the statistical distributions of residual (remaining) cross sections. This will be achieved through the use of microscopy images processed through *ImageJ* for void identification, combined with a *MATLAB* script for size estimations to give statistical values for cross section reduction. Based on the identified size of voids, their statistical distribution and the sample size, an expected failure load distribution is created based on the size of the weakest link. The predicted distribution will then be compared with experimental tensile test data for parts in PLA to estimate the accuracy of the proposed method.

2 Theory and background of fused deposition modelling

The basic concept of FDM is manufacturing through deposition of materials in the form of small strips of filament.

Usually, this is done by using thermoplastics, which are heated up to above-melting temperature and extruded through a nozzle onto a table or the workpiece as seen in Fig. 2 and Fig. 3. The base material is either supplied as continuous filament through a rolling wheel feeder or as pellets using a hopper and a reciprocating screw. The material is deposited layer by layer in the *z*-direction, using a 2.5 axis CNC system.

As the material is deposited as lines—rather than melting or curing of volumetric pixels—the material characteristics are highly dependent on the strategy for producing these segments. In general, the resulting parts' structural integrity is governed by five characteristics:

- *Strategy*—How are the filament paths placed?
- *Material*—What are the characteristics of the extruded base material?
- *Geometry*—How are these lines shaped?
- *Accumulated strain*—What strains have been introduced to the part throughout the process?
- *Inter filament bonding characteristics*—How well do these lines stick to other lines?

The production strategy and material are preset control parameters, while the geometry of the lines of filament, their accumulated strains and their bonding are variables, resulting
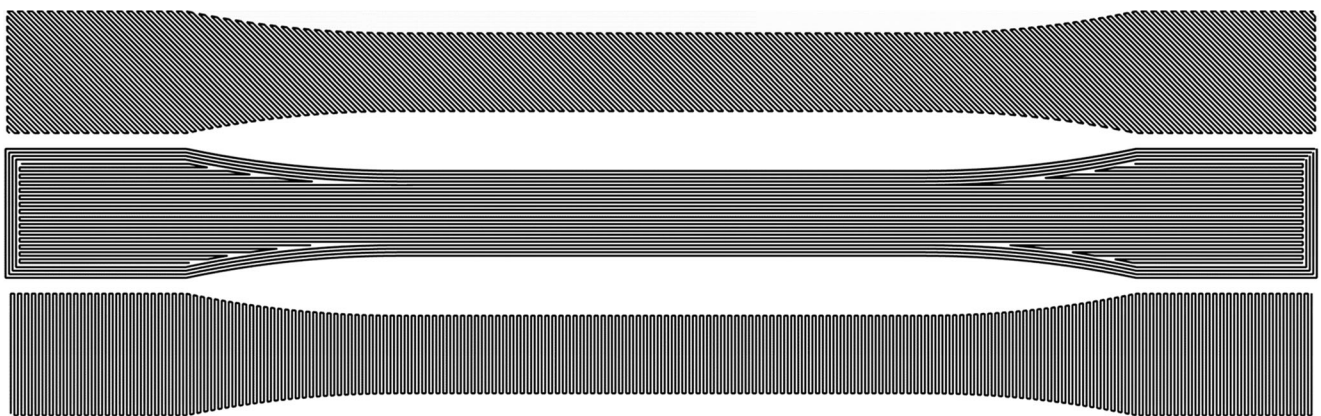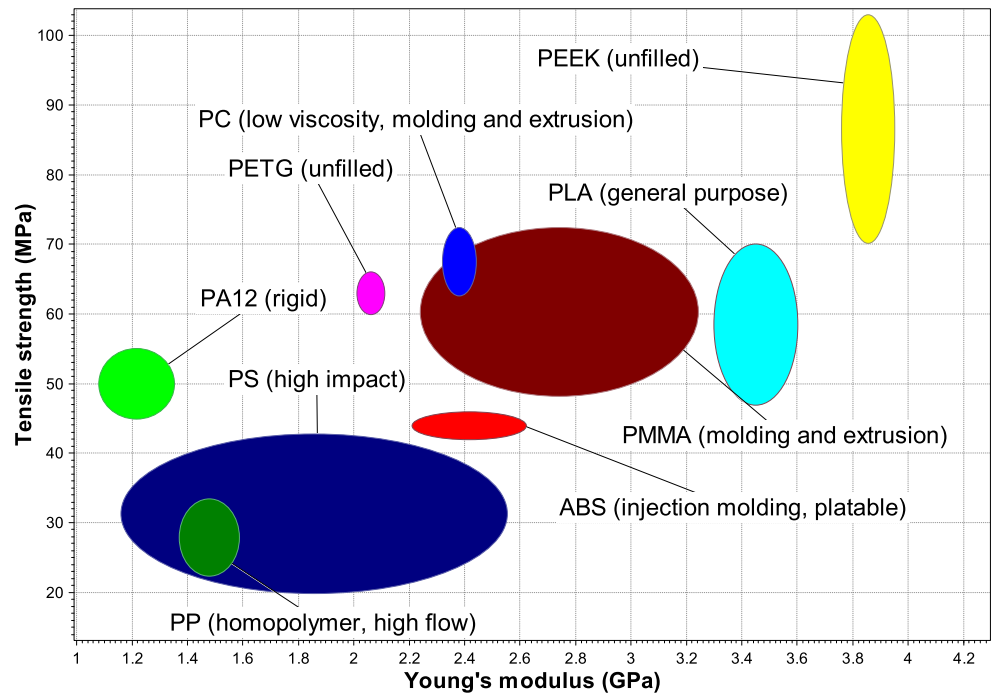

Fig. 5 45° (diagonal), 0° (longitudinal) and 90° (transverse) directed infill. 0° directed infill is shown printed with four outlines to reduce stress concentrations along the edges on the specimen exterior

Fig. 6 Tensile strength vs. Young's modulus for already in-market FDM materials. Data from the software CES EduPack from Granta Design Limited

from the process parameters as layer height, nozzle temperature, bed temperature, extruder multiplier, overlap, material, etc. One would often need to choose a strategy both for creating exterior or interior (infill) of a part and what mechanical and aesthetic properties these domains should have. The exterior is divided into four sub categories: the outline (the in-plane outward facing domain), the bottom (domain in contact

with build plate), the overhang or bridges (facing downwards into the air, or onto support structure), the top (facing out of *z*-plane upwards), as seen in Fig. 4.

To create a smooth outer surface, the outline is very often comprised of semi-continuous lines (lines that bite their tail), while the inner 2D domains are filled to their specified density. This can be achieved using different geometric patterns, e.g.,

Fig. 7 Fracture toughness vs. elongation to failure for already in-market FDM materials. Data from the software CES EduPack from Granta Design Limited
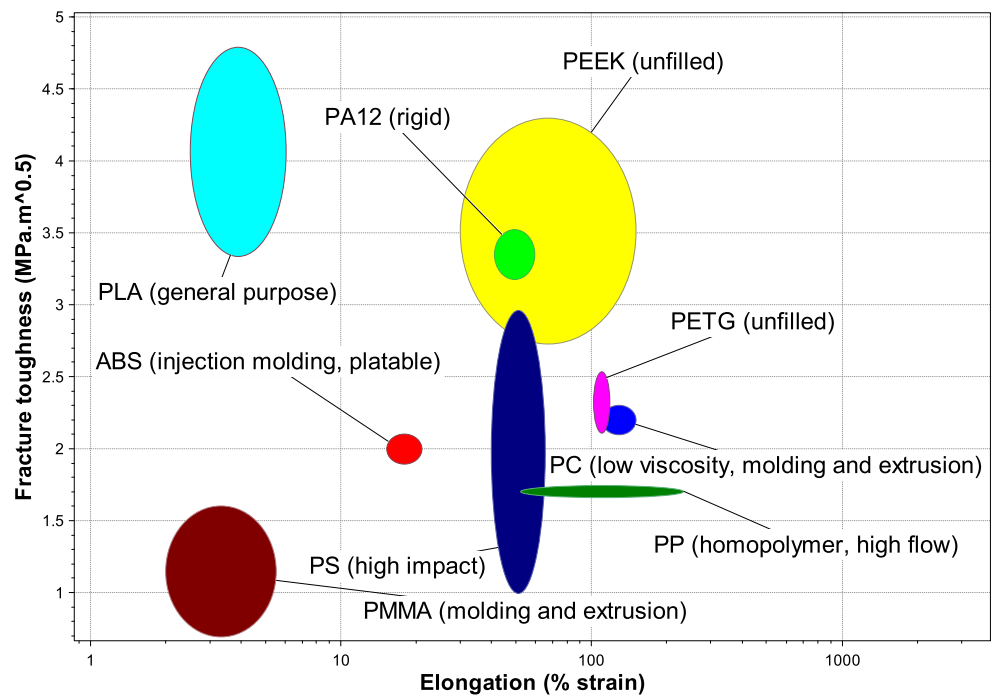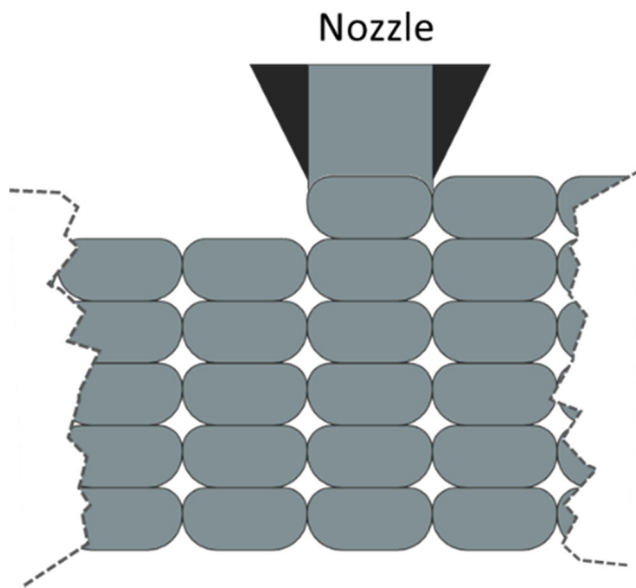
Fig. 8 Void formation between filaments

Fig. 10 Geometric measures of voids

linear raster, honeycomb, Hilbert curve or concentric raster, to create a near solid, or a partially filled structure to reduce density/material and cost/build time.

The prior research on the subject of material mechanics is mainly done using linear raster infill [4–6, 10, 11, 17], where efforts have been made to find the optimal infill types and orientations, or use the results for classical laminate theory. The reasons for not using more complex infill could be that it would involve more complex analysis, or the fact that this was the standard method of filling before honeycomb and cubic infill became mainstream. The common findings are, however, that compressive strength is not severely affected by infill direction, unlike the tensile strength which is highly dependent. The most used tensile test specimens are 0° (longitudinal) infill, ±45° and 90° angled (transverse) infill compared to the axis of loading, shown in Fig. 5. Research on ABS shows that specimens with transverse infill have the
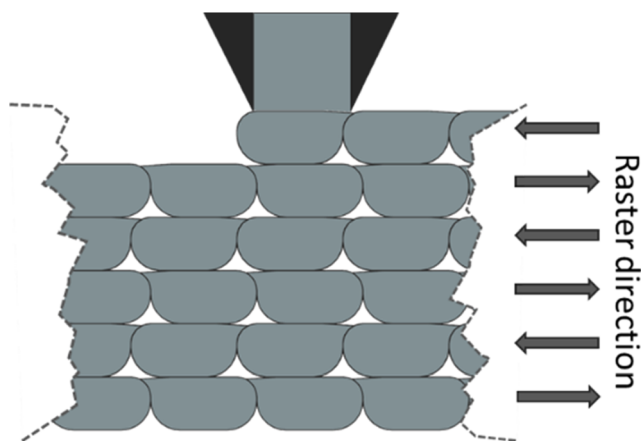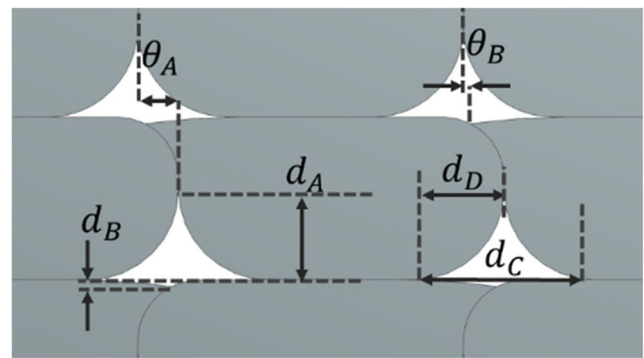
lowest performance, with a reported degradation of tensile strength from 22 to 90% [4, 6] compared to the bulk material. Some work using PLA reports an 8–16% reduction of strength of transversal specimens compared with longitudinal ones [18, 19]. However, this work seems to suffer from print quality issues and specimen printing orientations requiring support structures, which might have influenced the results. Specimens that are printed out of x-y plane are often omitted, possibly due to the non-symmetric manufacturing conditions. When creating on-bed standing tensile specimens, the temperature history, the vibrations and thereby the specimen characteristics would vary along its length. Especially voids tend to be smaller close to the heat bed than further away [20].

Many different materials are available on the market; a selection of them, alongside some of their mechanical properties, can be seen in Fig. 6 and Fig. 7. These could be provided as pure, copolymer or filled (carbon/glass/wood/silica), where the most used materials are unfilled PLA and unfilled ABS. Here, the dominant one is PLA due to its relatively low melting point and low shrinkage from solidification to room temperature, which make it easy to use for FDM. Compared with ABS, PLA has very good strength, stiffness and fracture toughness, but low elongation properties make it less suited
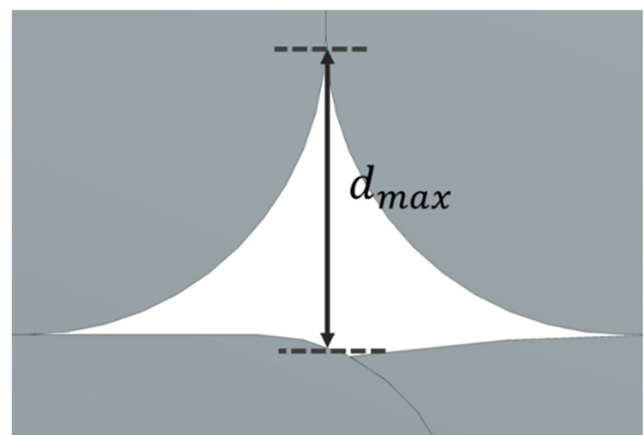

Fig. 9 Near triangular voids in zigzag pattern

Fig. 11 Size and position of the maximum vertical measure of a void, which will be used later in the paper

Table 1 Process characteristics for production of specimens

Layer height	0.3 mm
Extrusion multiplier	1.0
Nozzle temperature	210 °C
Heat bed temperature	55 °C
Print speed	60 mm/s
Nozzle size	0.4 mm

for components that utilise the material for springs and spring-like components (e.g., snap fits).

3 Anisotropy and voids

Extruded filament lines have a cross section spanning from oval to a near flattened appearance, where the main drivers for the geometry are:

- Flow rate
- Path placement
- Fluid/solid mechanics of the material
- Layer height

The origin of the shape can partly be explained from fluid mechanics, and the circular shape of the nozzle as Hagen–Poiseuille flow through the nozzle should be expected, using viscous materials such as molten plastics. This implies that the velocity of the material through the nozzle is highest at the centre and declining toward the nozzle wall. This, along with the circular shape of the nozzle, results in less extruded material away from the centreline of the extrusion path (or said otherwise, it would be difficult to extrude a perfectly rectangular line of molten material using a circular nozzle). In addition, the filament is commonly extruded into a corner made up by the previous layer and the previous line of filament, constraining the flow of material and hence flattening its boundaries. As these cross sections do not form sharp corners, placing many filaments alongside each other creates an almost uniform pattern of voids, as illustrated in Fig. 8.

How these voids form, depending on process characteristics, and their effect on mechanical behaviour has been investigated by Rodriguez et al. [6, 7]. Their findings show that the
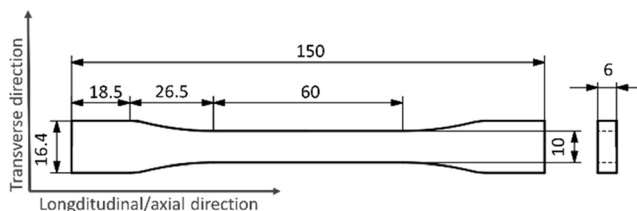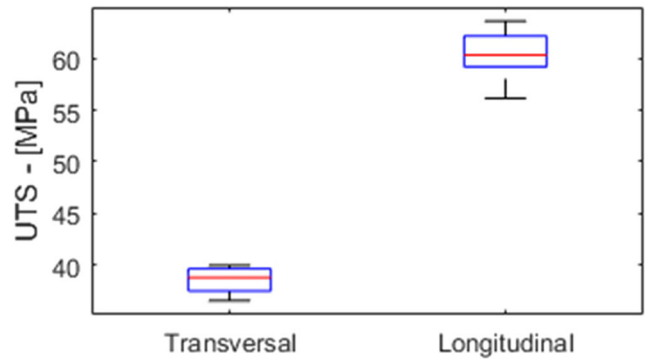

Fig. 13 Ultimate tensile engineering stress for the samples using cross section area based on its exterior dimensions

strength increases with decreased void sizes. Moreover, these voids are not rhombic but tend to extend more upwards than downwards, forming a kite/diamond shape. Some researchers report contradicting findings to this, however, suggesting that the voids extend less upward than downward [21, 22], attributed to, e.g., gravitational forces. However, our experience is in accordance with Rodriguez et al. [7], i.e., the observed asymmetry increases with increased flow rate or overlap of paths. High flow rate or overlap results in near triangular voids, alternating raster directions spread into a zigzag pattern as illustrated in Fig. 9.

We have defined the following geometric values, as measured from the layer boundary or filament boundaries, also shown in Fig. 10 and Fig. 11:

d_A maximum upwards extension of void
d_B maximum downwards extension of void
d_C maximum horizontal measure of void
d_D distance from left contact point to position of d_A
d_{max} maximum vertical measure of void
θ_A misalignment of filament intersections
θ_B misalignment of maximum upwards and downwards measure

Other geometric measures that have a significant effect on fracture behaviour would be the corner radii.
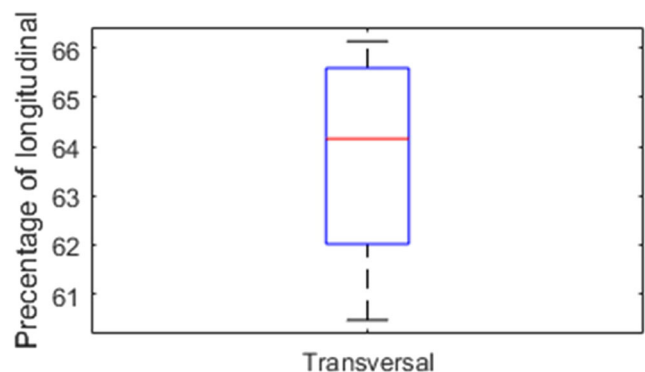

Fig. 12 Tensile specimen geometry

Fig. 14 Results from the transversal specimens compared with the mean of the longitudinal ones
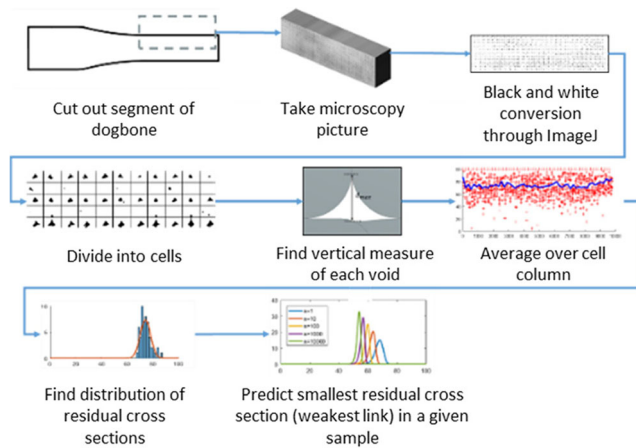
Fig. 15 Approach for analysis of residual cross section

How these voids form, or more correctly, how the bonds between filaments form, have been investigated by many researchers as this is a major factor to the strength of FDM parts. Li et al. [21] used geometric considerations to calculate the void density and bond geometry. Bellehumeur et al. [20] modelled the bond formation between two filaments, depending on temperature, while Sun et al. [13] investigated the temperature profile for some printing processes and its effect on void formation. Coogan and Kazmer [23, 24] modelled the strength of single filament-to-filament bonds, including the contribution of the reduced cross section, and effects of diffusion of polymer chains.

These efforts mainly sought to increase the understanding of the phenomenon of void/bond formation. When expanded to handle more complicated parts than single filament-to-filament bond, they could be of high value for predicting part strength. However, the approaches lack the stochastic perspective that would need to be incorporated for investigating real-world applications and performances. As noted by Gurralla and Regalla, the void sizes are not consistent [25], and a deterministic approach would therefore be insufficient.

To fill this gap, we would explore the statistical effect of void size distribution on ultimate tensile strength of transversely printed FDM parts. Our hypothesis is that it is possible to predict with reasonable accuracy the performance of a transversely printed specimen, compared to a longitudinally printed one, from the distribution of the maximum vertical measure of voids, and hence the distribution of residual cross

sections along the specimen. We further assume that the residual strength of the specimens compared with the ultimate tensile strength of the material is proportional to the estimated residual cross section compared with the net cross section. It is worth noting that the researchers mentioned above have mainly used ABS for their investigations, whereas we will use PLA in this study.

There are other theoretical models for describing fracture due to inherent voids, where the most widespread one is probably the Gurson model [26]. The essence of this model is that it describes the role of hydrostatic pressure in nucleation and growth of voids, hence explaining the pressure dependency of some materials. However, this model is mainly applicable for materials with ductile behaviour. This could exclude PLA, which is reported as brittle [27–29], typically worsened by ageing and exposure to moisture [30]. Also, because the voids are not randomly distributed, but regularly structured holes running across the whole cross section, the Gurson model would need extensive modification to work for FDM specimens.

Another approach for predicting the strength of FDM-printed specimens could be through linear elastic fracture mechanics (LEFM), as the voids mentioned could be seen as subcases of periodic notches/holes [31]. Notably, methods for estimating the stress intensity factors for closely placed rhombic holes with sharp edges, based on numerical calculations, are developed, e.g., the work of Savruk and Kazberuk [32]. Research has also been done on fracture toughness of FDM parts [8, 19]. However, using this as a predictive approach—i.e., investigating the development of cracks between each single void—LEFM would need sufficient control over the critical stress intensity factors in each domain of the tensile specimen. This would be difficult due to highly non-consistent thermal history and hence crystallinity and other material parameters [33].

It is worth noting that our method is not intended to describe the fundamental material mechanics around the voids, but rather to work as an engineering assessment of what to expect from FDM-printed parts due to reduction in residual cross section. Understanding the impact of this factor would be crucial for further investigating the influence of other phenomena such as diffusion of polymer chains, fracture mechanics and residual strain.

Fig. 16 Microscopy picture of dimensions 2570 × 724 compiled of three individual pictures
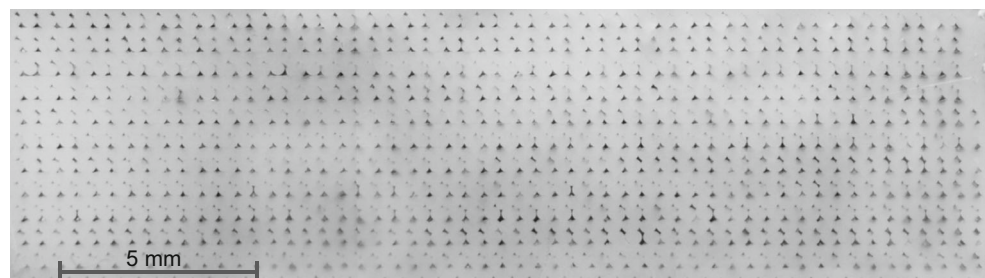
Fig. 17 Different threshold methods tried out, from upper left corner—Sauvola, Phansalkar, Otsu, Niblack, Midgrey, Median, Mean, Contrast and Bernsen. Auto local threshold method, with local radius of 200 pixels

4 Printing, tensile testing and microscopy preparation of samples

First, a total of eight transversely printed and eight longitudinally printed samples were made simultaneously in an unmodified Prusa i3 MK2 printer, with the process specifications given in Table 1.

To keep the research as scientifically controlled as possible (introducing few polymer additives), while maintaining it relevant for most practitioners, uncoloured PLA filament with a 1.75-mm diameter was chosen for the experiment. The PLA was stored in vacuum until printing and tested 2 days after printing, where stored in an air tight container.

A dog bone geometry based on *ISO 527-2-1B* was employed (as seen in Fig. 12), but its clamp section was made 16.4 mm wide (compared with the standard 20 mm clamp section) to make it fit into the clamps of the tensile test bench. The lay-up was equal to the 0° and 90° specimens in Fig. 5.

All samples were tested under quasi-static conditions with a displacement rate of 0.2 mm/min. An assortment of the results is seen in Fig. 13 and Fig. 14. The average ultimate tensile stresses (UTS) were 38.5 and 60.4 MPa for the transversal and longitudinal specimens, respectively, with standard deviations of 1.2 and 2.4 MPa.

The failure load of the transversal specimens falls in between 61 and 66% compared with the mean UTS of the longitudinally printed specimens. As the latter failed in the rounded fillet, possibly affected by stress concentrations inherent to the production method (from the discrete stepping seen in

Fig. 5, also noted by Ahn et al. [4]), these could have failed prematurely.

5 Method and analysis

The proposed method will aim to find the residual cross section through microscopy images of a segment of the tensile specimens. The strategy employed is summarised in Fig. 15.

One segment of a single, transversely printed specimen was cut along its centre axis, sanded and polished for inspection. Before inspection, the specimen was treated with dye penetrant for contrast enhancing, however avoiding dye penetrant extractor (white fluid used for extracting dye penetrant, and hence improve the visibility of cracks and defects) as this tends to give a misleading geometry/size of voids.

Three individual microscopy images of the sample were taken and combined, giving a total sample length of 29 mm and a resolution of 2570 × 724 pixels. Due to global colour gradients (colour differences not due to voids but miscolouring), a simple global greyscale threshold for identifying the voids would lead to misinterpreting the sizes of voids. Therefore, the image was processed through *ImageJ* using the *Auto Local Threshold* algorithm, which estimates the suitable threshold of each pixel based on the colour of the pixels within a radius of 100 pixels. There are different methods for deciding the threshold level, where the *Contrast* method captured the voids more accurately, i.e., giving the largest voids without
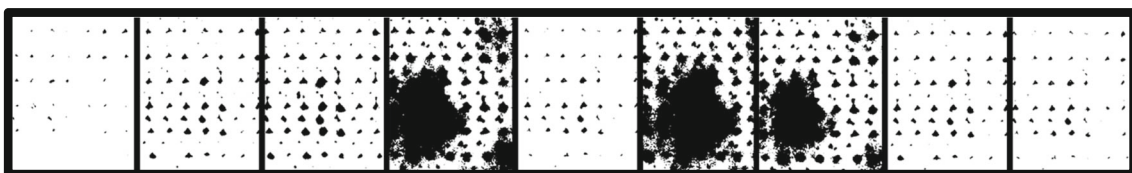

Fig. 18 Detail of same area with, from left to right—Sauvola, Phansalkar, Otsu, Niblack, Midgrey, Median, Mean, Contrast and Bernsen

exhibiting unnatural artefacts, and was therefore used in the rest of the study (see Figs. 16, 17, and 18).

The image was then divided into cells, containing one "filament intersection" each, as shown in Fig. 19. Each cell was scanned to identify the vertical pixel column in the cell with the highest number of black dots (finding d_{max}^{ij}, where ij denotes the row/column index of the cell), assuming this value to be constant throughout the cross section. The residual cross section factor (r^{ij}) of each cell was then taken as:

$$r^{ij} = 1 - \frac{d_{\max}^{ij}}{d_{\text{cell}}} \qquad (1)$$

where d_{cell} is the height of the cell. These values were then averaged over the column of cells, creating an average residual cross section factor for each column (R^j), as shown in Fig. 20. Using equal cell heights, R_j is calculated as:

$$R^j = \sum_{i=1}^{n} \frac{r^{ij}}{n} \qquad (2)$$

where n is equal to the number of rows in the specimen. This is the factor assumed to be proportional to the ultimate strength of a single cross section, based on the gross cross section of the specimen divided by the strength of the bulk material.

Referring to the measures from Fig. 19, the gross cross section of the specimen (A_{gross}) and the residual cross section (A_{res}) for each column j read:

$$A_{\text{gross}} = W \cdot H \qquad (3)$$

$$A_{\text{res}} = A_{\text{gross}} \cdot R^j \qquad (4)$$

The approach allowed for the maxima of voids in each cell column to be horizontally misaligned to some extent without affecting the results. This implies that triaxiality was neglected since this is difficult to incorporate without considering more complex analysis, such as finite element analysis (FEA).
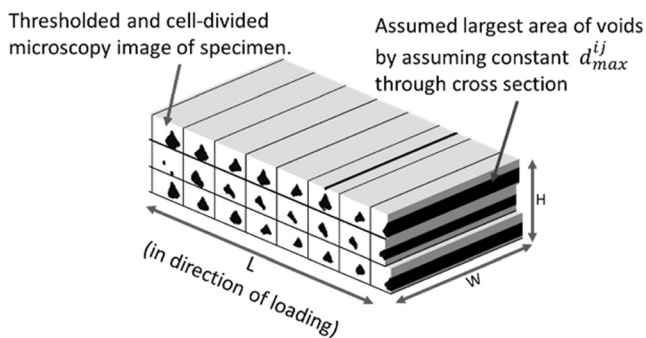

Fig. 19 Detail of the cell division of the black and white picture, together with the assumed geometry of the voids through the cross section. Cells are shown sliced at $d_{\max}$
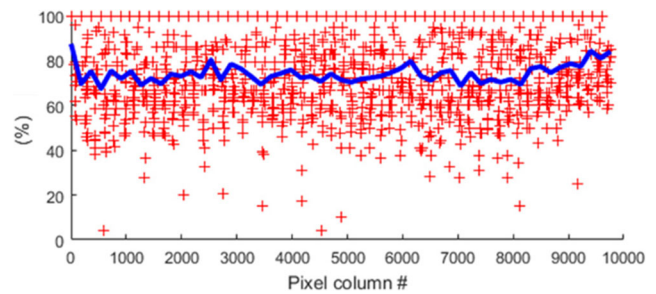

Fig. 20 The magnitude and position of each cell residual cross section fraction (r^{ij}) shown as red crosses, and average over whole column of cells (R^i) shown as blue line

The next step was then to estimate the weakest link W, representing the minimum residual cross section from a given sample size:

$$W = \min_{j=1 \to m} R^j \qquad (5)$$

where m is the total number of columns in a given sample. When estimating the weakest link in a sample size, and not the specimen, it is necessary to incorporate a statistical perspective. The general procedure is assuming a Gaussian distribution of the residual cross-sectional factors and finding the distribution of the expected weakest link within a sample. An approximative Gaussian distribution, using mean and standard deviation from the distribution of the residual cross sections, from a microscopy picture, is shown in Fig. 21.

Denoting the probability density function (PDF) for the residual cross section factors and the cumulative distribution function f_R and F_R, respectively, these provide the following relationship:

$$F_R = \int_0^x f_R \, \mathrm{dx} \qquad (6)$$

The cumulative distribution function (CDF) for the probability of the weakest link in a sample of size m would then be the following:

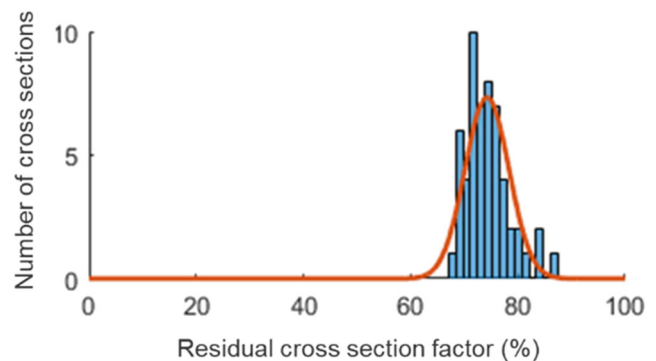$$F_W^m = 1 - (1 - F_R)^m \qquad (7)$$

Fig. 21 Real distribution of residual cross section minimums, alongside the probability density function of standard Gaussian distribution scaled to the same numbers of samples

which is a Weibull distribution, often seen in weakest link problems. Moreover, its associated probability density function is:

$$f_W^m = \frac{d}{dx} F_W^m \tag{8}$$

This gives the probabilities for a sample of arbitrary size m and print quality equal to the printed specimens, shown in Fig. 22.

It is observed that as the sample size grows large, alongside its decreasing value of the weakest link, the variance decreases, as shown in Fig. 23. This should make the failure load estimations more correct for larger samples. Due to the weakest link effect, the distribution shows a steeper decline than incline, indicating very low probability of a high strength outcome. As a "rule of thumb", for this print quality and size in the range of 100 lines of filament, it would be unlikely for a specimen to achieve a strength of more than 70% of the strength of a void free sample.

6 Comparison with experimental tensile test data

The above probability values are all compared to a solid cross section. Hence, to compare it to longitudinally printed ones, this must be scaled accordingly as these also exhibit cross-sectional reduction. As voids for longitudinally printed
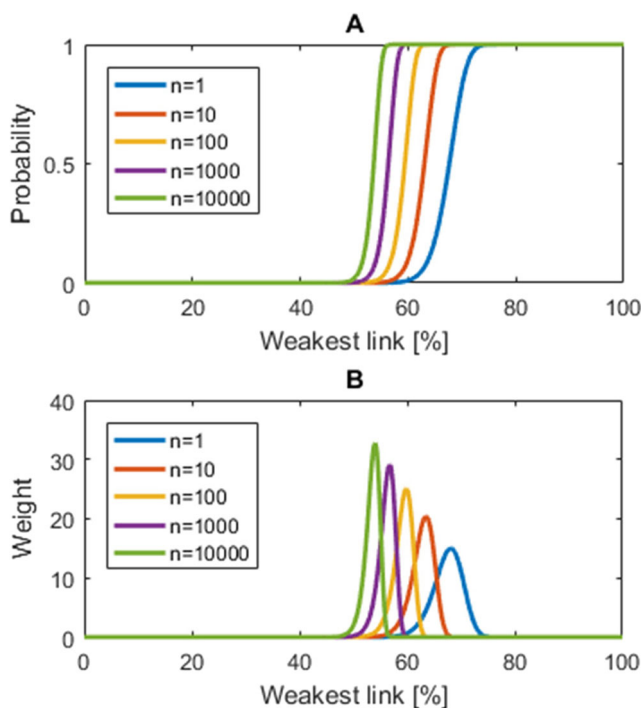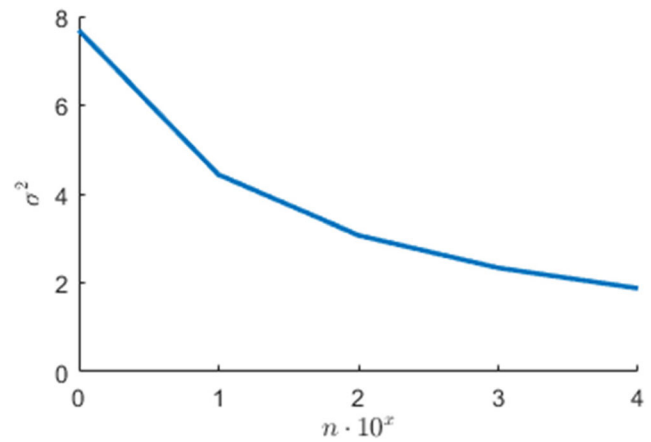
Fig. 23 Variance as function of sample size

specimens run along the axis of loading, the volume fraction would be a sufficient scaling factor. Estimating the volume fraction from the microscopy picture, yields $v_f = 0.9525$. Also, the print strategy used on the transverse specimens results in a wavy surface on its edges as shown in Fig. 24 (where the nozzle changes direction), which collocates with the cross-section minimums. An average over 15 "valleys" result in a reduction in cross-sectional area of 5.8% (denoted $\varepsilon_{\text{edges}}$), and variation in this measure is neglected.

The test samples had a straight section of 60 mm, which results in $m = 150$ filament lines, when using a line width of 0.4 mm. Moreover, it is assumed that tensile failure would arise when the axial stress in the weakest link reaches a critical level and that this level is the same as for the longitudinal printed specimens. Formally, this can be stated as:

$$\frac{F_{\text{transverse}}}{A_{\text{gross}} \cdot W \cdot (1 - \varepsilon_{\text{edges}})} = \frac{F_{\text{longitudinal}}}{A_{\text{gross}} \cdot v_f} \tag{9}$$

Under the above assumptions, this yields the probability density function and cumulative distribution function for the ultimate tensile strength shown in Fig. 25 and Fig. 26.
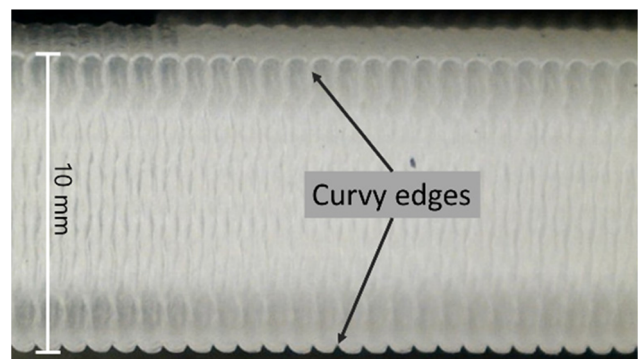
Fig. 22 **a** Cumulative distribution function. **b** Probability density function for the weakest link in a sample of size n, in percentage of a solid cross section

Fig. 24 Curvy edges on the sides of the transversely printed specimens, narrowing the specimen at the locations of maximum void concentrations
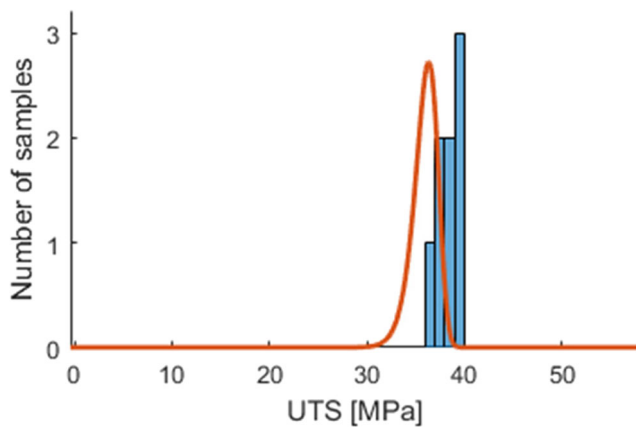
Fig. 25 Scaled probability density function (continuous line) for model alongside experimental data (bars) for ultimate tensile stress using gross cross section (calculated from exterior dimensions of the specimen) of the transversely printed specimens

For our data, the model gives a close yet slightly conservative estimate (about 5 MPa discrepancy) and a matching shape of the continuous distribution.

7 Discussion, limitations and further work

The method proposed herein gives a close estimate on the expected distribution of failure loads of transversely printed specimens based on the failure load of longitudinally printed specimens. However, in this case, the method predicts a lower outcome than the physical experiments. As the approach neglects incomplete atomic diffusion and fracture mechanics, it would lead one to assume that the estimate would predict a higher strength than the physical experiments. The discrepancy could be explained by possible premature failure of the longitudinally printed specimens due to stress concentrations in the fillets of the tensile samples. The residual cross section
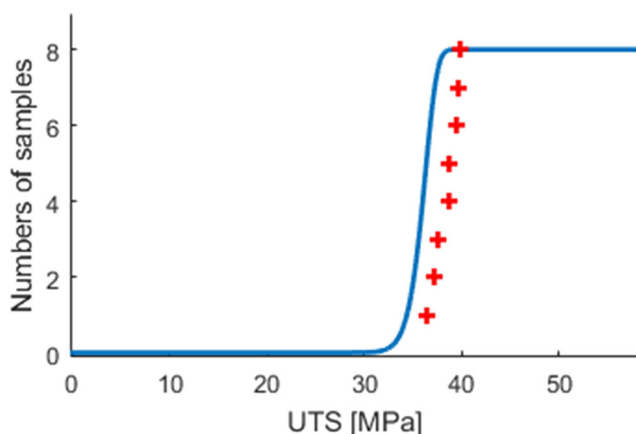

Fig. 26 Scaled cumulative distribution function (continuous line) for model alongside experimental data (markers) for ultimate tensile stress using gross cross section for the transversely printed specimens

estimation method using a series of microscopy pictures could also be the origin of this under-prediction of strength.

However, according to our proposed model, there is reason to believe that for specimens of PLA, much of the anisotropic behaviour could be explained directly by the reduction in residual cross section. Due to this effect, the probability of achieving a relatively high strength sample diminishes fast with increased specimen length.

The proposed method is only suitable for the prediction of failure loads for transversely printed specimens. Also, our method is only assessed for PLA, which is the dominant material in practitioner's usage, although less used in previous research.

The method should be further verified by design of experiment techniques, such as Taguchi methods or factorial design, to investigate the influence of different printing conditions on the void sizes and position, and whether the resulting voids can explain the changes in tensile capacity. This approach could also be validated for different printing orientations, or for finding the influence of void sizes on other capacity measures such as ultimate compressive strength and ultimate shear strength.

Another important aspect that should be investigated is the through-thickness properties of the voids. The element of stress triaxiality and fracture could also be investigated, using, e.g., FEA and experimental fracture toughness tests. The mentioned aspects would all be important for future application of this model, whose ultimate aim is to link the bulk material properties and the structural properties of a printed part.

Publisher's Note Springer Nature remains neutral with regard to jurisdictional claims in published maps and institutional affiliations.

References

1. Tronvoll SA, Elverum CW, Welo T (2017) Prototype experiments: strategies and trade-offs. Procedia CIRP 60:554–559
2. Wohlers T. (2016) Wohlers report 2016. Wohlers Associates, Inc.
3. Chen L, He Y, Yang Y, Niu S, Ren H (2017) The research status and development trend of additive manufacturing technology. Int J Adv Manuf Technol 89:3651–3660
4. Ahn S, Montero M, Odell D, Roundy S, Wright PK (2002) Anisotropic material properties of fused deposition modeling ABS. Rapid Prototyp J 8:248–257

5. Ahn SH, Baek C, Lee S, Ahn IS (2003) Anisotropic tensile failure model of rapid prototyping parts—fused deposition modeling (FDM). Int J Mod Phys B 17:1510–1516

6. Rodríguez JF, Thomas JP, Renaud JE (2001) Mechanical behavior of acrylonitrile butadiene styrene (ABS) fused deposition materials. Experimental investigation. Rapid Prototyp J 7:148–158

7. Rodriguez JF, Thomas JP, Renaud JE (2000) Characterization of the mesostructure of fused-deposition acrylonitrile-butadiene-styrene materials. Rapid Prototyp J 6:175–186

8. Torres J, Cotelo J, Karl J, Gordon AP (2015) Mechanical property optimization of FDM PLA in shear with multiple objectives. JOM 67:1183–1193

9. Torres J, Cole M, Owji A, DeMastry Z, Gordon AP (2016) An approach for mechanical property optimization of fused deposition modeling with polylactic acid via design of experiments. Rapid Prototyp J 22:387–404

10. Sood AK, Chaturvedi V, Datta S, Mahapatra SS (2011) Optimization of process parameters in fused deposition modeling using weighted principal component analysis. J Adv Manuf Syst 10:241–259

11. Casavola C, Cazzato A, Moramarco V, Pappalettere C. Materials & design 2016;90:453–458

12. Mahmood S, Qureshi AJ, Goh KL, Talamona D (2017) Tensile strength of partially filled FFF printed parts: experimental results. Rapid Prototyp J 23:122–128

13. Sun Q, Rizvi GM, Bellehumeur CT, Gu P (2008) Effect of processing conditions on the bonding quality of FDM polymer filaments. Rapid Prototyp J 14:72–80

14. Chacón JM, Caminero MA, García-Plaza E, Núñez PJ (2017) Additive manufacturing of PLA structures using fused deposition modelling: effect of process parameters on mechanical properties and their optimal selection. Mater Des 124:143–157

15. Liu X, Zhang M, Li S, Si L, Peng J, Hu Y (2017) Mechanical property parametric appraisal of fused deposition modeling parts based on the gray Taguchi method. Int J Adv Manuf Technol 89:2387–2397

16. Thrimurthulu K, Pandey PM, Venkata Reddy N (2004) Optimum part deposition orientation in fused deposition modeling. Int J Mach Tools Manuf 44:585–594

17. Panda SK, Padhee S, Sood AK, Mahapatra SS (2009) Optimization of fused deposition modelling (FDM) process parameters using bacterial foraging technique. Intell Inf Manag 01:89–97

18. Letcher T, Waytashek M (2014) Material property testing of 3D-printed specimen in PLA on an entry-level 3D printer, ASME 2014; IMECE2014–39379

19. Song Y, Li Y, Song W, Yee K, Lee K-Y, Tagarielli VL (2017) Measurements of the mechanical response of unidirectional 3D-printed PLA. Mater Des 123:154–164

20. Bellehumeur C, Li L, Sun Q, Gu P (2004) Modeling of bond formation between polymer filaments in the fused deposition modeling process. J Manuf Process 6:170–178

21. Li L, Sun Q, Bellehumeur C, Gu P (2002) Composite modeling and analysis for fabrication of FDM prototypes with locally controlled properties. J Manuf Process 4:129–141

22. Wang J, Xie H, Weng Z, Senthil T, Wu L (2016) A novel approach to improve mechanical properties of parts fabricated by fused deposition modeling. Mater Des 105:152–159

23. Coogan TJ, Kazmer DO (2017) Healing simulation for bond strength prediction of FDM. Rapid Prototyp J 23:551–561

24. Coogan TJ, Kazmer DO (2017) Bond and part strength in fused deposition modeling. Rapid Prototyp J 23:414–422

25. Gurrala PK, Regalla SP (2014) Part strength evolution with bonding between filaments in fused deposition modelling. Virtual Phys Prototyping 9:141–149

26. Gurson AL et al (1977) Continuum theory of ductile rupture by void nucleation and growth: Part I—Yield criteria and flow rules for porous ductile media. J Eng Mater Technol 99:2–15

27. Todo M, Park S-D, Takayama T, Arakawa K (2007) Fracture micromechanisms of bioabsorbable PLLA/PCL polymer blends. Eng Fract Mech 74:1872–1883

28. Todo M, Shinohara N, Arakawa K (2002) Effects of crystallization and loading-rate on the mode I fracture toughness of biodegradable poly(lactic acid). J Mater Sci Lett 21:1203–1206

29. Arakawa K, Mada T, Park S-D, Todo M (2006) Tensile fracture behavior of a biodegradable polymer, poly(lactic acid). Polym Test 25:628–634

30. Kim E, Shin Y-J, Ahn S-H (2016) The effects of moisture and temperature on the mechanical properties of additive manufacturing components: fused deposition modeling. Rapid Prototyp J 22:887–894

31. Pilkey WD (1997) Holes. In: Peterson's stress concentration factors. John Wiley & Sons, Inc., Hoboken, pp 175–376

32. Savruk MP, Kazberuk A (2009) Stresses in an elastic plane with periodic system of closely located holes. Mater Sci 45:831–844

33. Park S-D, Todo M, Arakawa K (2005) Effects of isothermal crystallization on fracture toughness and crack growth behavior of poly(lactic acid). J Mater Sci 40:1055–1058